

HIGH EFFICIENCY DYE SENSITIZED SOLAR CELLS BY EXCITATION OF LOCALIZED SURFACE PLASMON RESONANCE OF AGNPs

^{1,3*} Eli, D. and ² Gyuk, P. M.

¹ Department of Physics, Nigerian Defence Academy, Kaduna, Nigeria.

² Department of Physics, Kaduna State University, Kaduna, Nigeria.

³ Department of Physical Sciences, Greenfield University, Kaduna, Nigeria

* Corresponding Author's Email Address: danladielibako@gmail.com

Phone: +2348063307256

ABSTRACT

Noble metal particles have demonstrated significant potential in solar energy technologies which is attributed to their enhanced capability in light-harvesting, due to the plasmonic effects. The systematic design and formation of plasmonic dye sensitized solar cells (DSSCs) by integrating Ag@TiO₂ core-shell nanoparticles (NPs) in two distinct configurations; on top of the TiO₂ and on the FTO transparent substrate were reported. The plasmonic effects were investigated systematically. The most efficient configuration is obtained by incorporating Ag@TiO₂ NPs with a simple architecture of FTO/c-TiO₂/m-TiO₂/AgNPs@TiO₂ which results to increase in power conversion efficiency (PCE) from 0.071 % to 0.384 %, demonstrating ~5.45 times enhancement, compared with the reference device without the metal NPs. The enhancement is attributed to the increase in light harvesting due to increased optical path length caused by light scattering of metallic nanostructures. This strategy demonstrates a novel structure to enhance the performance of photovoltaic device.

Keywords: DSSCs, AgNPs@TiO₂, Surface Plasmon, Natural Pigment.

INTRODUCTION

Solar energy technologies have the potential to cater for problems associated with both global environment and energy; this is because "Energy from sunlight that reaches the Earth in one hour alone is more than all of the energy consumed by humans in an entire year (Jun *et al.*, 2013). For the past decades, dye sensitized solar cells have received significant interest owing to their cost effectiveness and potential of overcoming energy crisis. However, increasing power conversion efficiency further to realize the outdoor applications are still one of the crucial issues in DSSC research.

Metal nanoparticles have been found to be employed as promising materials to enhance the performance of solar cells (Eli *et al.*, 2019; Eli *et al.*, 2016; Alfagiannis *et al.*, 2012; Isah *et al.*, 2016; Onimisi *et al.*, 2016; Wang *et al.*, 2011), acting as scattering centers and sub-wavelength antennas (Xiahou *et al.*, 2018).

It is worth mentioning that for noble metal nanoparticles to have significant positive effect in solar cells, the non-radiative transfer between the photoactive layer and nanoparticles must be reduced (Wang *et al.*, 2011). The noble metal nanostructures effect depends on the size, shape, component, and dielectric environment of the materials (Eli *et al.*, 2016; Luo *et al.*, 2017;

Zhang *et al.*, 2013). Metal nanoparticles exhibit localized surface plasmon resonances (LSPR) that couple strongly to the incident light. As it has been reported (Isah *et al.*, 2016; Luan & Wang, 2014), that the surface plasmon effect is caused by light-driven collective oscillations of conduction electrons in metallic nanoparticles, and the nanoparticles must be smaller than the wavelength of exciting light for electrons to oscillate with the electric field of light. When these conditions are met, an enhanced electromagnetic field is found near the surface of the nanoparticles (Luan & Wang, 2014).

Reports on plasmonic applications in DSSCs focused on integration of metal nanoparticles within the mesoporous metal oxide or the charge transport layers to improve device performance (Matsubara & Tatsuma, 2007). In 2016, Isah *et al.*, recorded an efficiency enhancement of about 50 % when silver nanoparticles were incorporated into mesoporous layer of solar cell, leading to an increase from 0.18 to 0.27 % in PCE. The device performance enhancement was attributed to plasmon-mediated hot carrier injection from AgNPs to titanium dioxide. Also, our previous studies, (Eli *et al.*, 2016) demonstrated a dramatic increase in DSSC by incorporating two SILAR cycles of AgNPs in cell's active layer and it results to: (i) 63% improvement in efficiency, (ii) 48.4% enhancement in short circuit current density and (iii) 8.5% improvement in open circuit voltage over the bare fluorine doped tin oxide (FTO)-based device lacking AgNPs. The increase of *J*_{sc} was attributed to the enhanced dye light absorption in strength and spectral range due to the surface plasmon resonance of AgNPs in photo anode, while the increase of *V*_{oc} may be related to the more negative level of the quasi-Fermi energy of Ag-TiO₂ composite system resulting from the added AgNPs. Also in 2017, Eli *et al.*, also reported the performance of plasmon assisted dye sensitized solar cells capped with SiO₂ and TiO₂ based on natural pigment and the enhancement of ~2.8 times in photocurrent was recorded with the SiO₂ capping. When TiO₂ was used, an increase of ~1.0 times was recorded. In the case of SiO₂ capping, the enhancement in photocurrent is exclusively attributed to the influence of LSP effect. However, in the case of films containing coated TiO₂, both charging and LSP are in play. The higher photocurrent essentially arises from the improved charge separation and increased absorption of the incident light which suggests that charging effects seen in cell with TiO₂ capping seem to minimize the plasmonic influence in the DSSC. Also, the cell with TiO₂ capping undergoes charge equilibration with the neighbouring TiO₂ NPs which in turn assists in maintaining a more negative Fermi level.

In 2013, it was demonstrated by Guo *et al.*, that inclusion of AgNPs into solar cell to trap and confine light could give a superior performance. They recorded an enhancement of about 34 % which was attributed to the increase in light harvesting due to the light scattering of the metallic nanostructures. In 2012, Lin *et al.*, fabricated solar cells with Plasmonic structures of FTO/TiO₂/NPs-Ag and FTO/NPs-Ag/TiO₂ electrodes. In the FTO/TiO₂/NPs-Ag, a 60 % enhancement in photocurrent and an improvement in photovoltage were observed. However, the photovoltaic properties of the FTO/NPs-Ag/TiO₂ were similar to those of the standard electrode.

In metallic nanostructures based DSSCs, it is essential to avoid direct contact between metallic nanostructures and liquid electrolyte, (Cui *et al.*, 2016; Yuan *et al.*, 2015) because that leads to charge recombination and exciton quenching loss at the surface of metallic nanostructures (Lee *et al.*, 2016; Choi *et al.*, 2013; Zhang *et al.*, 2013).

Previous works reported the use of Ag@SiO₂ to prevent corrosion and recombination (Eli *et al.*, 2016; Choi *et al.*, 2012), others demonstrated the use of Ag@TiO₂ and Ag@PVP was demonstrated (Xu *et al.*, 2012) but no literature has demonstrated the use of TiO₂ as core shell with silver nanoparticles deposited on nanocrystalline TiO₂ blocking layer to minimize carrier leakage on bare FTO with natural pigment. Therefore, it is very critical to systematically study the positive effects of using in-plane surface plasmon (SP) nanoparticles (NPs) of silver coated on both the top and the bottom of a m-TiO₂ semiconductor with TiO₂ capping to observe/investigate how easily the shell can transfer electrons to the surrounding porous m-TiO₂, which may facilitate the development of DSSCs toward outdoor applications.

In this work, we developed a new and efficient plasmonic composite structure to effectively enhance the PCE of DSSCs by incorporating AgNPs on top m-TiO₂ porous layer with a TiO₂ capping. Anthocyanins pigment from *Hibiscus Sabdariffa* was then used as the sensitizer in a sandwich type DSSCs. The choice of anthocyanin is due to its requisite hydroxyl functional groups (-OH) to bind better to the TiO₂ surface while maintaining a short distance between the dye skeleton and the point connected to TiO₂ surface. The addition of Ag@TiO₂ NPs increased the rate of exciton generation and the probability of exciton dissociation, thereby enhancing the short-circuit current density and the PCE in both configurations.

MATERIALS AND METHODS

Synthesis of Ag nanoparticles

To fabricate the silver NPs, a modified two-step reduction synthesis procedure was implemented, which was developed based on the conventional reduction method (Nourolahi *et al.*, 2016; Agnihotri *et al.*, 2014). We first heat the mixture containing sodium borohydride (NaBH₄) and tri-sodium citrate (TSC) at the ratio of 2:7 (1x10⁻³ mol dm⁻³: 3.5x10⁻³ mol dm⁻³) to 60 °C at 300 rpm for 30 min under vigorous stirring to ensure a formation of homogenous solution. 45 min later, 4 ml of an aqueous solution of AgNO₃ (4x10⁻³ mol dm⁻³) was added drop-wise to the mixture, and the temperature was further raised to 100°C to make the solution boil quickly. The reaction was allowed to continue for another 45 min. Finally, the solution was cooled down to room temperature

with stirring, and the NPs were collected by centrifugation at 5000 rpm and redispersed in ethanol via sonication for 15 min.

Preparation of the Natural Dye

The flowers of *Hibiscus Sabdariffa* were harvested and air dried till they became invariant in weight. The method of heating in water was used to extract the dye as previously demonstrated in our studies (Eli *et al.* 2016). Distilled water was the solvent for aqueous extraction. 50 g of the sample (Dried *Hibiscus Sabdariffa*) was measured using analytical scale and dipped in 50 ml of the solvent heated to 100°C for 30 min after which solid residues were filtered out to obtain clear dye solutions. The dye is rich in anthocyanin with a chemical structure containing cyanidin and delphinidin complex as shown in Fig. 1 (Onimisi *et al.*, 2016; Frank & Ciin, 2005, Terahara *et al.*, 1990).

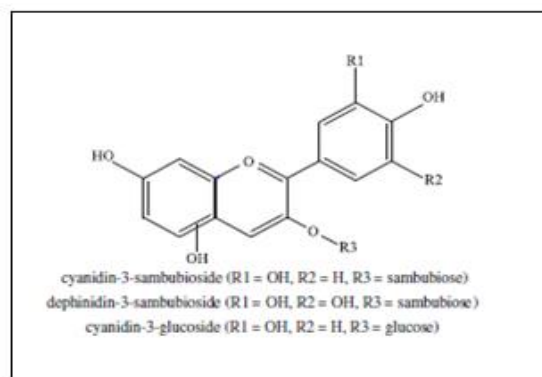


Fig.1. Chemical structures of: cyanidin and delphinidin in *Hibiscus Sabdariffa*

Device Fabrication and Assembly

The FTO conductive glass sheets were washed with laurylsulphate then later rinsed with water six times in an ultrasonication bath for 10 min, then finally washed in isopropanol. We utilized successive ionic layer adsorption and reaction (SILAR) and screen printing method to achieve two different design strategies.

Normally, the mesoporous TiO₂ layers used in DSSC devices often contain small holes that allow direct contact between the electrolyte and conducting electrode and result in the charge leakage. In order to prevent the carrier leakage, a blocking layer has been used between the conducting electrode and the mesoporous TiO₂ layer.

The photoanode was prepared by depositing the blocking layer on the FTO conductive glass sheets, followed by the mesoporous titanium dioxide (TiO₂) The blocking layer was deposited from a 2.5 wt% TiO₂ precursor and was applied to the FTO glass substrate by spin coating and subsequently sintered at 450°C for 40 min (Eli *et al.*, 2016). The TiO₂ layer was deposited by screen printing. It was then sintered in air for 30 mins at 500°C. The silver was deposited on top and bottom surface of the TiO₂ with one SILAR cycle that has thickness of about 56 nm (At this point, we utilized ISolution Image Analysis programming to measure the size of Ag nanoparticles) through successive ionic layer adsorption and reaction.

To ensure the silver was protected against chemical attack by the electrolyte that will etch up the SPR effect, TiO₂ of thin layer ~7 μm was deposited on the Ag using spin coating method with sodium silicate (Na₂SiO₃) as the precursor. The counter electrode was prepared by screen printing a platinum catalyst gel coating onto the FTO glass. It was then dried at 100°C and fired at 450°C for 30 min.

The sintered photo anodes were sensitized by immersion in the sensitizer (anthocyanin pigment) solution at room temperature for 12 hours.

The DSSCs photo anodes and the screen printed-Pt counter electrodes were assembled to form a solar cell by sandwiching a redox (tri-iodide/iodide) electrolyte solution. The electrolyte solution consists of 2 m L acetonitrile, 0.1 M propylene carbonate, 0.005 M LiI, 0.0005 M I₂. Therefore, the open side of the cell assembly was sealed properly with epoxy resin gum (Eli et al., 2017).

Characterization and Measurement

The current density-voltage (*J-V*) characteristics of the cells were recorded using a setup comprising a xenon lamp, an AM 1.5 light filter, and an Electrochemical Analyzer (Keithley 2400 source meter) under an irradiance of 100 mW/cm² illumination from a Newport A solar simulator. Scanning electron microscopy (SEM) images were obtained using Carl Zeiss at an acceleration voltage of 20 kV. Visible region extinction spectra of dye, electrodes without dye and electrodes with dye were recorded on Axiom Medicals UV752 UV-vis-NIR spectrophotometer. The cell active area was 0.25 cm².

RESULTS AND DISCUSSION

Fig. 2, shows the SEM images of FTO/c-TiO₂/m-TiO₂, FTO/c-TiO₂/AgNPs@TiO₂/m-TiO₂, and FTO/c-TiO₂/m-TiO₂/AgNPs@TiO₂. The SEM surface morphology of the reference electrode is shown in Fig. 2a. The SEM image shows little difference between films with randomly two dimensional array of AgNPs with a wide range of size (57 nm). All films showed compact morphologies and smooth surfaces with shining surface which is a representation of the catalytic and scattering ability of AgNPs.

Fig. 3a. represents the UV-vis of the natural dye at specific wavelength (350-800 nm). The dye was observed to absorb best at a peak of 550 nm which ascertain the presence of anthocyanin which also meets its demand for used as light harvester in this research.

The UV-vis of the architecture of AgNPs deposited on top and bottom of c-TiO₂ before and after dye sensitization is depicted in Fig. 3b and c. It was observed that the enhancement is noticed in the dye loaded nanocomposite which indicates that in the presence of dye molecules, AgNPs absorb more photons than without dye. It was observed that the structure FTO/c-TiO₂/m-TiO₂/AgNPs@TiO₂, absorbs best at the peak of 410 nm and the structure FTO/c-TiO₂/AgNPs@TiO₂/m-TiO₂, absorbs at the peak of 390 nm. The reference electrode FTO/c-TiO₂/m-TiO₂ was observed to have two peaks, 480 and 540 nm as demonstrated in Fig. 3c.

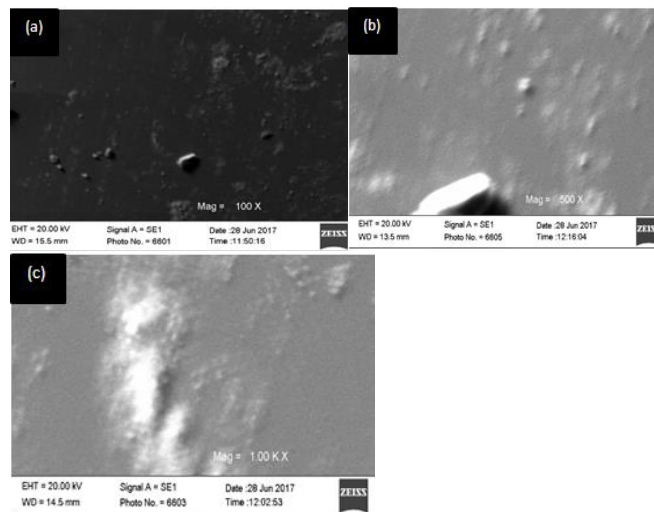


Fig. 2 SEM images of (a) FTO/c-TiO₂/ m-TiO₂, (b) FTO/c-TiO₂/AgNPs@TiO₂/m-TiO₂, and (c) FTO/c-TiO₂/ m-TiO₂/AgNPs@TiO₂

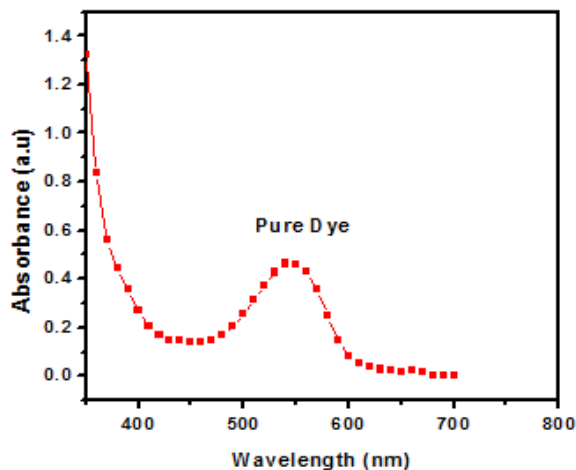


Fig. 3a. UV-Vis spectra of the dye

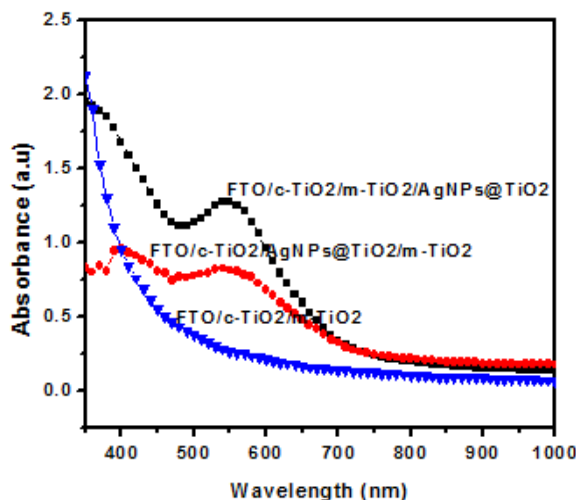


Fig. 3b. UV-vis spectra of various prepared Photoanodes before

dye sensitization

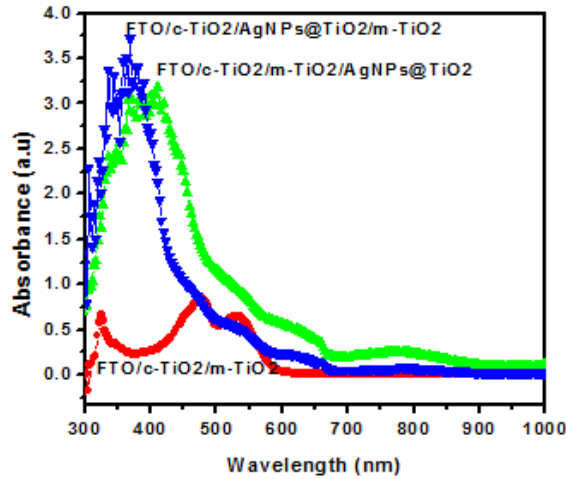


Fig. 3c. UV-vis spectra of various prepared Photoanodes after dye sensitization

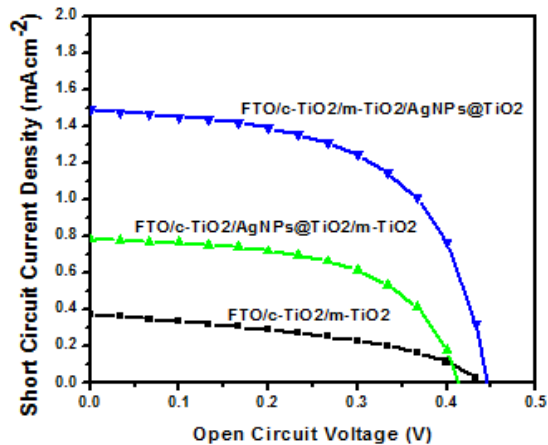


Fig. 4. Photocurrent density-voltage (J - V) curve under 100 mWcm^{-2} light intensity

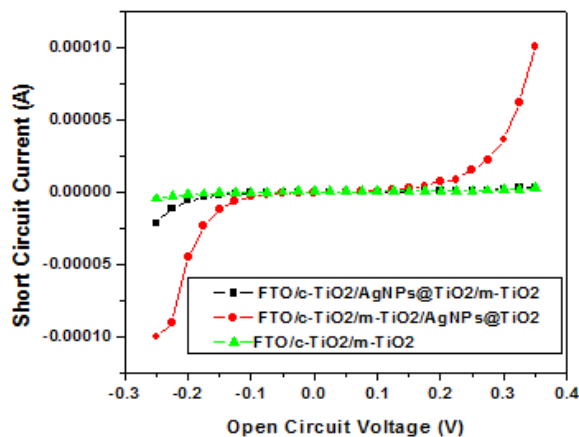


Fig. 5. J - V curve without illumination

Table 1: Photovoltaic performance of DSSCs with various photo anodes under 100 mWcm^{-2}

Sample	Photo anode	$J_{sc}(\text{mAcm}^{-2})$	$V_{oc}(\text{V})$	FF	$\eta(\%)$
1	FTO/TiO ₂	0.372	0.433	0.438	0.071
2	FTO/AgNPs@TiO ₂ /TiO ₂	0.780	0.412	0.576	0.185
3	FTO/TiO ₂ /AgNPs@TiO ₂	1.487	0.447	0.577	0.384

The typical J - V curves of DSSC devices with and without Ag@TiO₂ core-shell nanostructures are shown in Fig. 4. For the reference device without Ag@TiO₂ core-shell, the V_{oc} , J_{sc} and FF are 0.433 V, 0.372 mA/cm^2 , and 0.438, respectively, resulting in a PCE of 0.071 %. The cells photovoltaic parameters are summarized in Table 1.

The ideality factor and efficiency of the device were obtained from the J - V curve following equations (1) and (2) respectively (Eli et al., 2016):

$$FF = \frac{J_{max} \times V_{max}}{J_{SC} \times V_{OC}} \quad (1)$$

$$\eta = \frac{FF \times J_{SC} \times V_{OC}}{P_{IRRADIANCE}} \cdot 100\% \quad (2)$$

Where

FF is Fill Factor, η is solar cell efficiency, V_{max} is maximum voltage, J_{max} is maximum current density, J_{sc} is short circuit current density, V_{oc} is open circuit voltage and $P_{IRRADIANCE}$ is light intensity.

For maximizing the positive benefits of Ag@TiO₂ core-shell nanostructures for improving photovoltaic performance, J - V characteristics of DSSC devices incorporated Ag@TiO₂ nanostructures with two distinct configurations were examined respectively. For DSSC device with the configuration FTO/c-TiO₂/AgNPs@TiO₂/m-TiO₂, the V_{oc} , J_{sc} and FF are 0.412 V, 0.780 mA/cm^2 and 0.571, respectively, resulting in a PCE of 0.185 %. Changing the configuration to FTO/c-TiO₂/m-TiO₂/AgNPs@TiO₂, the DSSC device shows a PCE of 0.384 % with V_{oc} of 0.447 V, J_{sc} of 1.487 mA/cm^2 and FF of 0.577, respectively.

The above results suggest that Ag@TiO₂ core-shell nanostructures introduced into DSSCs could dramatically improve the performance of DSSCs, and the optimized structure is FTO/c-TiO₂/m-TiO₂/AgNPs@TiO₂. It is evident that the J_{sc} and η both increased with the addition of AgNP but highly significant with the configuration FTO/c-TiO₂/m-TiO₂/AgNPs@TiO₂.

DSSCs with AgNPs@TiO₂ modification show higher photovoltaic values than the control device without AgNPs@TiO₂ modification. The increase in the exciton generation rate and the exciton dissociation probability enhances free carrier generation/charge separation, reduces the recombination rate, enhances the carrier-transport-collection, and, therefore, improves the J_{sc} and η factors of plasmonic thin film solar cells.

The increment of J_{sc} in FTO/c-TiO₂/m-TiO₂/AgNPs@TiO₂ was attributed to the enhanced light absorption and broadened light absorption range of the dye resulting from the SPR of AgNPs,

which stimulated the dye to generate more charge carriers in the active layer and increases the probability of exciton generation and dissociation, leading to an increase of the photocurrent generation.

Due to the decay of a strong local magnetic field from the Ag surface on FTO/c-TiO₂/AgNPs@TiO₂/m-TiO₂ configuration, only fewer dye molecules were enhanced to promote charge separation. It caused an apparent decrease of the optical absorption of dye, resulting in a limited enhanced photocurrent. Also a smaller Schottky barrier in the interfacial region of Ag and semiconductor, attributed to a little difference between the work function of silver, 4.12 eV, and the electron affinity of TiO₂, 4.0 eV, had almost no influence on photocurrent in the visible region to match closely with the record for the standard electrode (Zhou *et al.*, 1996). Also the electrons from metal particle cannot efficiently be transported in the network and the scattering study showed that in this case specular reflectivity is maximized, thus preventing a fraction of light to penetrate the device while the light scattering to non-specular directions is not sufficient enough.

Notably, we found an enhanced region of charge separation of DSSCs, which was beneficial for promoting the charge separation of excited dye within the nanostructured TiO₂ film. The enhanced direction excited by surface plasmon of AgNPs is not toward collecting FTO, leading to unfavorably enhanced photovoltaic property for FTO/c-TiO₂/AgNPs@TiO₂/m-TiO₂.

Addition of AgNPs is thus seen to reduce the e-h recombination centers generally attributed to the oxygen vacancies in TiO₂ in the surface layers (Muduli *et al.*, 2012). Also, the Ag plasmon mode energetically overlaps with dye absorption zone possibly rendering charge into the TiO₂ nanoparticles (Du *et al.*, 2009). In our work, when AgNPs is deposited between m-TiO₂ semiconductor and anthocyanin pigment, the catalytic and scattering effect of AgNPs sited on TiO₂ support increased the rate of reaction between the TiO₂/dye and the triiodide/iodide electrolyte in the plasmon assisted DSSC, thereby diminishing the recombination probability. As a result, the electric field of the SPR that release hot oscillating electrons and quickly shuttled to another TiO₂ acceptor enhances the transport of generated excitons from excited dye to the TiO₂ semiconductor thereby giving better performance (Barazzouki & Hotchandani, 2004).

When AgNPs was coated at the bottom of the m-TiO₂ semiconductor, the light trapping and confinement of plasmonic structure does not affect dramatically the exciton separation of excited dye by near-field effect. The photovoltaic properties are not significantly enhanced because the enhanced direction in which the surface plasmon excited by AgNPs is the opposite of that toward collecting FTO conductive sheets which results to insignificant influence on the moving of regular photoelectrons. To further investigate the effect of AgNPs, the J-V characteristics of these solar cells were measured in the dark (Fig. 5) under forward bias. In this case, the plasmonic effect does not contribute to the overall characterization of the devices. Under the dark condition, there is no current flowing thereby behaving as a diode as depicted in Fig. 5. This rectifying behaviour is a feature of photovoltaic devices and is a consequence of the asymmetric junction needed to separate charges.

Conclusion

In the present work we compare the performance of DSSCs, based on anthocyanin pigment when silver nanoparticles (NPs) are incorporated in two distinct places among the device structure. Introduction of NPs on top of the blocking layer on the transparent anode revealed an improved performance with an increased efficiency of ~2.63 times to the reference electrode. Alternatively, placing the NPs on top of the active photovoltaic layer resulted to ~ 5.45 times higher efficiency compared to the reference electrode. The optimized structured device is obtained with the architecture of FTO/c-TiO₂/m-TiO₂/AgNPs@TiO₂. The plasmonic enhancement mechanism is associated with improved exciton generation rate, enhanced exciton dissociation probability as well as more efficient carrier transfer /collection induced by the LSPR effect

REFERENCES

- Agnihotri, S., Mukherji, S. & Mukherji, S. (2014). *RSC Advances*, 4, 3974–3983.
- Alfagiannis, K., Karagiannidis, P. G., Pitsalidis, C., Panagiotopoulos, N.T., Gravalidis, C., Kassavetis, S., Patsalas, P. and Logothetidis, S. (2012). *Solar Energy Materials & Solar Cells*, 104, 165–174.
- Barazzouk, S. & Hotchandani, S. (2004). *Journal of Applied Physics*, 96, 7744–7746.
- Choi, H., Chen, W. T. & Kamat, P. V. (2012). *ACS NANO*, 6(5), 4418–4427.
- Choi, H., Lee, J. P., Ko, S. J., Jung, J. W., Park, H., Yoo, S., Park, O., Jeong, J. R., Park, S. & Kim, J. Y. (2013). *Nano letters*, 13, 2204–2208.
- Cui, J., Chen, C., Han, J., Cao, K., Zhang, W., Shen, Y. & Wang, M. (2016). *Advanced Science*, 3, 1500312.
- Du, L., Furube, A., Yamamoto, K., Hara, K., Katoh, R. & Tachiya, M. (2009). *Journal of Physical Chemistry C*, 113, 6454–6462.
- Eli, D., Ahmad, M., Maxwell, I., Ezra, D., Francis, A. & Sarki, S. (2016). *Journal of Energy and Natural Resources*, 5(1), 11–15.
- Eli, D., Ibeh, G. J., Ige, O. O., Owolabi, J. A., Ugbe, R. U., Sherifdeen, B. O., Onimisi M. Y. & Ali, H. (2019). *Journal of Theoretical and Applied Physics*, 1(3), 88–98.
- Eli, D., Kassimu, A. A. & Oluwaseyi, B. S. (2017). *Journal of the Nigerian association of mathematical physics*. 43, 311–316.
- Eli, D., Onimisi, M.Y., Abdu, S. G., Gyuk, P.M. & Ezeoke, J. (2016). *Journal of Scientific Research & Reports*, 10(4), 1–8.
- Eli, D., Owolabi, J. A., Olowomofe, G. O. & Ezeoke, J. (2016). *Journal of Photonic Materials and Technology*, 2(1), 6–13.
- Eli, D., Owolabi, J. A., Olowomofe, G. O., Onimisi, M. Y. & Francis, A. (2016). *American Chemical Science Journal*, 14(3), 1–8.
- Frank, T. & Clin, J. (2005). *Pharmacol.* 2005, 45:203.
- Guo, K., Li, M., Fang, X., Liu, X., Sebo, B., Zhu, Y. & Zhao, Z. X. (2013). *Journal of Power Sources*, 230, 155–160.
- Isah, K. U., Jolayemi, B. J., Ahmadu, U., Kimpa, M. I. & Alu, N. (2016). *Materials for Renewable and Sustainable Energy*, 5, 10 pages.
- Jun, H.K., Careem, M.A. & Arof, A.K. (2013). *Renewable and Sustainable Energy Reviews*, 22, 148–167.
- Lee, D. S., Kim, W., Cha, B. G., Kwon, J., Kim, S. J., Kim, M., Kim, J., Wang, D. H. & Park, J. H. (2016). *ACS applied materials & interfaces*, 8, 449–454.

- Lin, S.-J., Lee, K.-C., Wu, J.-L. & Wu, J.-Y. (2012). *Solar Energy*, 86, 2600–2605.
- Luan, X. and Wang, Y. (2014). *Journal of Material Research and Technology*, 30, 1–7.
- Luo, Q., Zhang, C., Deng, X., Zhu, H., Li, Z., Wang, Z., Chen, X. & Huang, S. (2017). *ACS Applied Materials Interfaces*, 9 (40), 34821–34832.
- Matsubara, K. and Tatsuma, T. (2007). *Advanced Materials*, 19, 2802–2806.
- Muduli, S., Game, O., Dhas, V., Vijayamohan, K. Bogle, K. A., Valanoor, N. & Ogale, S. B. (2012). *Solar Energy*, 86, 1428–1434.
- Onimisi, M. Y., Eli, D., Abdu, S. G., Aboh, H. O. & Ezeoke, J. (2016). *American Chemical Science Journal*, 13(3), 1-8.
- Terahara, N., Saito, N., Honda, T. Tokis, K. & Osajima, Y. (1990). *Phytochemistry*, 29:949.
- Wang, D. H., Kim, D. Y., Choi, K. W., Seo, J. H., Im, S. H., Park, J. H., Park, O. O. & Heeger, A. J. (2011). *Angew. Chem. Int. Ed.* 50, 5519–5523.
- Xiahou, Z. S., Cao, T., Zhang, K., Wang, Z., Huang, P., Zhu, K., Yuan, L., Zhou, Y. Song, B., Xia, H. & Chen, N. (2018). *Organic Electronics*, 52, 309-316.
- Xu, Q., Liu, F., Meng, W. & Huang, Y. (2012). *Optics Express*, A898, 20(S6). 9 Pages.
- Yuan, Z., Wu, Z., Bai, S., Xia, Z., Xu, W., Song, T., Wu, H., Xu, L., Si, J., Jin, Y. & Sun, B. (2015). *Advanced Energy Materials*, 5, 1500038.
- Zhang, W., Saliba, M., Stranks, S. D., Sun, Y., Shi, X., Wiesner, U. & Snaith, H. J. (2013). *Nano letters*, 13, 4505- 4510.
- Zhao, G., Kozuka, H. & Yoko, T. (1996). *Thin Solid Films*, 277, 147–154